



Ion-beam deposited platinum as electrical contacting material in operando electron microscopy experiments at elevated temperatures

Simonsen, Søren Bredmose; Ma, Zhongtao; Mariegaard, Elisabeth; De Angelis, Salvatore; Dacayan, Waynah Lou; Mølhave, Kristian Speranza; Chatzichristodoulou, Christodoulos

Published in:
Microscopy Research and Technique

Link to article, DOI:
[10.1002/jemt.24373](https://doi.org/10.1002/jemt.24373)

Publication date:
2023

Document Version
Publisher's PDF, also known as Version of record

[Link back to DTU Orbit](#)

Citation (APA):
Simonsen, S. B., Ma, Z., Mariegaard, E., De Angelis, S., Dacayan, W. L., Mølhave, K. S., & Chatzichristodoulou, C. (2023). Ion-beam deposited platinum as electrical contacting material in *operando* electron microscopy experiments at elevated temperatures. *Microscopy Research and Technique*, 86(8), 1003-1011.
<https://doi.org/10.1002/jemt.24373>

General rights

Copyright and moral rights for the publications made accessible in the public portal are retained by the authors and/or other copyright owners and it is a condition of accessing publications that users recognise and abide by the legal requirements associated with these rights.

- Users may download and print one copy of any publication from the public portal for the purpose of private study or research.
- You may not further distribute the material or use it for any profit-making activity or commercial gain
- You may freely distribute the URL identifying the publication in the public portal

If you believe that this document breaches copyright please contact us providing details, and we will remove access to the work immediately and investigate your claim.

Ion-beam deposited platinum as electrical contacting material in *operando* electron microscopy experiments at elevated temperatures

Søren Bredmose Simonsen¹  | Zhongtao Ma¹ | Elisabeth Mariegaard¹ |
Salvatore De Angelis¹ | Waynah Lou Dacayan¹ | Kristian Speranza Mølhavé² |
Christodoulos Chatzichristodoulou¹

¹DTU Energy, Kgs. Lyngby, Denmark

²DTU Nanolab, Kgs. Lyngby, Denmark

Correspondence

Søren Bredmose Simonsen, DTU Energy,
Fysikvej, Kgs. Lyngby, Denmark.
Email: sobrs@dtu.dk

Funding information

H2020 European Research Council,
Grant/Award Number: 850850

Review Editor: Alberto Diaspro

Abstract

Establishing a stable and well conducting contacting material is critical for *operando* electron microscopy experiments of electrical and electrochemical devices at elevated temperatures. In this contribution, the nanostructure and electrical conductivity of ion beam deposited Pt are investigated both in vacuum and in oxygen as a function of temperature. Its microstructure is relatively stable up to a temperature of approx. 800°C and up to an applied current density of approx. 100 kA/cm². Its conductivity increases with temperature, attributed to densification, with changes in the hydrocarbon matrix being less important. Recommendations are provided with respect to the Pt deposition parameters in terms of maximizing stability and minimizing electrical resistance.

Research Highlights

- It is feasible to use ion beam deposited Pt as electrical contacting material in *operando* electron microscopy.
- The deposited Pt is relatively stable up to 800°C and approx. 100 kA/cm².
- The resistivity can be reduced by increasing the applied ion current during deposition and by thermal annealing at a temperature of 500°C in a few mbar of oxygen.

KEYWORDS

conductivity, electrical measurements, ion-beam deposited Pt, *operando* electron microscopy, resistance

1 | INTRODUCTION

In electron microscopy, in-situ and *operando* methods are becoming increasingly more important. In particular, in transmission electron microscopy (TEM), the introduction of Micro Electronic Mechanical

System (MEMS) chip-based holders has led to the rapid development of methodologies allowing to directly relate structure and composition with material functionality (Alam et al., 2020; Allard et al., 2009; Creemer et al., 2010; Gaulandris et al., 2020; Mele et al., 2016; Niekietal et al., 2017; Vijayan & Aindow, 2019; Yokosawa et al., 2012; Zheng

This is an open access article under the terms of the [Creative Commons Attribution-NonCommercial-NoDerivs](https://creativecommons.org/licenses/by-nc-nd/4.0/) License, which permits use and distribution in any medium, provided the original work is properly cited, the use is non-commercial and no modifications or adaptations are made.

© 2023 The Authors. *Microscopy Research and Technique* published by Wiley Periodicals LLC.

et al., 2022; Zintler et al., 2017). MEMS chips are also employed in conjunction with scanning electron microscopy (SEM) for in-situ and *operando* experiments (Mølhave et al., 2004; Schwarzbach et al., 2019).

One important class of in-situ/*operando* experiments involves electrical measurements, yielding the electrical or electrochemical response of materials/devices with nanoscale dimensions (Alam et al., 2020; Haas et al., 2019; Kamaladasa et al., 2015; Zheng et al., 2022). Such experiments have given insight into, for example, solid state battery dynamics (Basak et al., 2022; Hammad Fawey et al., 2016; Wang et al., 2020; Yang et al., 2016; Zhang et al., 2022). With the use of combined heating-biasing holders, such measurements can be performed as a function of temperature (Schwarzbach et al., 2019). In a recent study, we showed that by combining the heating-biasing chips with an environmental TEM (ETEM) it is possible to perform reliable electrochemical impedance spectroscopy (EIS) measurements of solid oxide cell components in the TEM (Ma et al., 2023).

For electrical measurements, it is crucial to ensure sufficient electrical contact between the sample and the current collecting pads of the MEMS chip. To realize this, lithography methods are sometimes used to deposit a conducting material connecting the sample with the MEMS chip (Seeger et al., 2001; Evans et al., 1978). Another method is ion-beam (IB) or electron-beam (EB) deposition using a focused ion beam SEM (FIB-SEM) (Zhong et al., 2020). An advantage of this approach is that the sample can be mounted precisely on the MEMS chip with a micro-manipulator while using the IB to deposit the conducting and connecting material, as well as for further thinning and adjusting the sample and contact geometry.

Materials that are commonly available for IB deposition in a FIB are Pt (Puretz & Swanson, 1992; Tao et al., 1990), C (Van Leer et al., 2009), and W (Gamo et al., 1986; Xu et al., 1989). Other metals such as Au (Blauner et al., 1989; Ro et al., 1987), Pd (Gross et al., 1986), Al (Gamo et al., 1984), Cu (Della Ratta et al., 1993), Fe (Furuya, 2008), Ta (Gamo et al., 1986), as well as insulators, e.g. SiO₂ (Komano et al., 1989), and tetraethoxysilane (TEOS) (Young & Puretz, 1995) are also used. For electrical measurements in vacuum and at RT, all metals can be used for contacting. For experiments at elevated temperature, a thermally stable material must be employed. Here, C, W, Ta, Pt and Pd are the best candidates. If the in-situ experiment is performed in a gas phase (e.g., in an ETEM), an inert contacting material is required. For high temperature experiments performed in an oxidizing gas, materials that easily oxidize cannot be used, which excludes C, W, Ta, Al, Cu, Fe, and to some extent Pd. Accordingly, Pt stands out as the most versatile contacting material and seems to be the best candidate for in-situ/*operando* experiments in oxidizing gases at elevated temperatures. For these reasons, this work focuses on Pt as electrical contacting material.

IB- and EB-deposited Pt has a complex nanostructure with a mixture of Pt nanoparticles and partly decomposed Pt-containing hydrocarbon species from the precursor (Tao et al., 1990; Zhong et al., 2020). The Pt-to-hydrocarbon ratio depends on the deposition conditions, with increasing Pt content upon increasing IB current (Tao et al., 1990). For EB deposition, the Pt content is typically lower (Protochips, 2017). For IB deposition, the material will also contain ions from the FIB source (e.g., Ga, Ar, Xe, etc.).

The deposition method and conditions impact the conductivity of the deposited material. Tao et al. reported that the resistivity of IB deposited Pt increases 10³ times (from approx. 70 to 70 mΩ cm) when decreasing the beam current by a factor of 10 (from 222 to 22 pA) (Tao et al., 1990). The resistivity of EB-deposited Pt is generally even higher, with reported values varying within a factor of 10³ from approx. 4 mΩ cm (Protochips, 2017) to approx. 1 Ω cm (Zhong et al., 2020). Both IB- and EB-deposited Pt have much higher resistivity compared to bulk Pt (approx. 0.1 μΩ cm), making it challenging to carry out resistivity measurements of highly conductive materials. Since IB-deposited Pt has higher conductivity compared to EB-deposited Pt, this is usually the best choice as a contacting material. Only in cases that require minimal overspray of the deposited Pt, it can be necessary to use EB deposition (Hammad Fawey et al., 2016).

In the present study, we investigate the conductivity of IB-deposited Pt as a function of temperature, up to 900°C where instability of the contacting material was observed. The experiments are carried out both in vacuum and in 2 mbar of O₂ in an ETEM, to study the possible influence of an oxidizing gas environment. In addition, the relation between the applied current and internal Joule heating of the Pt is described. Finally, we investigate the effect of a thermal oxidation pre-treatment to remove the hydrocarbon precursor from the IB-deposited Pt to form a pure metallic Pt contacting material.

2 | METHODS

2.1 | Ion-deposition

Pt was IB-deposited on commercial MEMS heating-biasing chips (DENS solutions). The conditions for the various depositions are presented in Table 1. In all cases, the precursor C₅H₄CH₃Pt(CH₃)₃ (purchased from Zeiss) was used.

2.2 | Microscopy and electrical measurements

Imaging and electrical measurements were conducted in a Crossbeam 1540XB SEM with a field-emission gun (ZEISS), a TM3000 SEM

Acronym	Ion	Voltage (kV)	Current (pA)	Thickness (nm)	In-situ condition
GaPt	Ga	30	20	80	2 mbar O ₂
ArPt	Ar	30	200	200	Vacuum
XePt	Xe	30	300	200	Vacuum

TABLE 1 Ion beam deposition conditions, deposition thickness and conditions for the in situ experiment.

(ZEISS) with an Quantax EDS detector (Bruker), and a Titan 80–300 ETEM (Hansen et al., 2009). TEM images were recorded at 300 kV using a OneView Camera (Gatan). SEM images were recorded with the Crossbeam at 10 kV using an Everhart Thornley Detector and with the TM3000 at 15 kV using a backscatter detector.

For experiments in vacuum, the heating and electrical polarization were performed using a Keithley Model 2450 and the Impulse software (DENS solutions). The MEMS chips were connected to the Keithley via a Lightning heating-biasing TEM holder or an in-situ FIB stub in the FIB-SEM (both DENS solutions). Four probe measurements were conducted by applying a constant current in steps up to 2 mA while measuring the voltage from which the resistance was calculated.

For the ETEM experiment, a Gamry FAS2 Femtostat was connected to the TEM holder. Two-point electrochemical impedance spectroscopy (EIS) was conducted within the frequency range 0.1–10⁵ Hz and amplitude of 20 mV. The method of combining EIS with ETEM for nanoscale samples in gasses and elevated temperatures has recently been described in detail (Ma et al., 2023). The resistance was obtained from the analysis of Nyquist plots. For comparison, linear sweep voltammetry (LSV) in the range 0–5 mV was also conducted and the resistance was extracted from the slope. The measured resistances from EIS and LSV were almost identical and only the values from EIS are presented in the following analysis. The ETEM experiments were performed in 2 mbar O₂.

For all experiments, the temperature was ramped stepwise. Imaging and electrical measurements were performed while keeping the temperature constant. For the TEM analysis, the temperature ramping rate was 100°C/min while for SEM it was 3°C/min. To minimize the influence of the electron beam, the sample was only exposed when images were recorded, blanking the beam otherwise.

The resistivity and conductivity are calculated from the resistance by using the sample geometries. Here, the inner distance between the chip electrodes is used as the sample length. The width is measured from the SEM or TEM images. For the ETEM experiment, the Pt was deposited on the approx. 20 nm thick electron transparent SiN window. An approximately 80 nm thick Pt film was deposited in the center enforced by thicker layers (approx. 130 nm) on the sides. The thicknesses were measured using electron energy loss spectroscopy (EELS). For SEM experiments, the Pt was deposited on the 400 nm thick SiN support membrane. In this case, EELS measurement was not possible, due to the large total thickness, and the indicated Pt film thicknesses (Table 1) are the expected values according to the chosen deposition parameters.

3 | RESULTS AND DISCUSSIONS

3.1 | Conductivity at room temperature

Figure 1 presents SEM images of the deposited Pt films connecting the electrodes on commercial MEMS chips for in-situ/*operando* microscopy (deposition parameters described in Table 1). In this work, the Ar IB deposited Pt is not perfectly uniform and cavities or holes

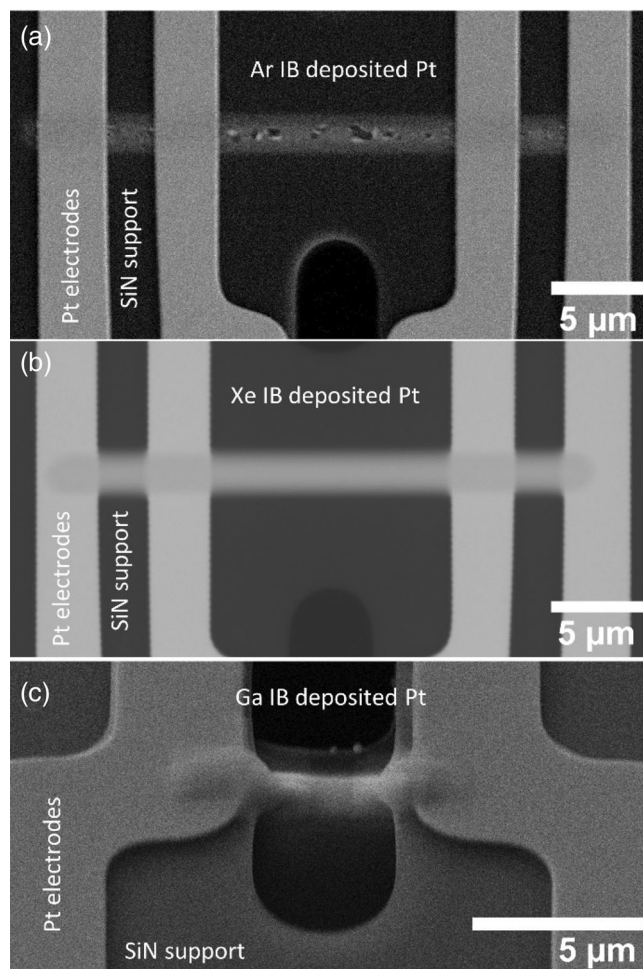


FIGURE 1 SEM images of MEMS chips with (a) Ar, (b) Xe and (c) Ga IB deposited Pt films.

are observed (Figure 1a). On the contrary, the Xe and Ga ions give a more uniform deposition (Figure 1b,c). The inhomogeneity will result in a larger uncertainty when calculating the resistivity from the measured resistance because the Pt film geometry is less well-defined.

Figure 2 presents the resistivity and conductivity as a function of ion current for the IB deposited Pt (deposition parameters described in Table 1). Generally, the conductivity increases as a function of the ion current, and this trend is consistent with a previous report from Tao et al. (1990).

The resistivities of the IB deposited Pt films are 10³–10⁵ times higher than that of metallic Pt. According to Bruggeman's model the conductivity for a porous material, σ_{por} depends on the conductivity of the bulk material, σ_{bulk} , the volume fraction of the conducting phase, ε and the tortuosity, τ in the following way (Tjaden et al., 2016):

$$\sigma_{\text{por}} = \sigma_{\text{bulk}} \frac{\varepsilon}{\tau}$$

The equation shows that the conductivity of the porous material is controlled by structural factors. Increasing porosity or tortuosity will

decrease the conductivity. The relatively low conductivity for the IB deposited Pt according to Figure 2 is partly due to its porous nature with tortuosity values greater than 1. The deposited Pt may even, to some degree, consist of poorly connected Pt islands on the basis of previously reported nanostructures for EB deposited Pt (Zhong et al., 2020).

3.2 | Conductivity as a function of temperature

The temperature of IB deposited Pt (Figure 1a, ArPt in Table 1) was elevated in the high vacuum of an SEM ($<10^{-5}$ mbar). Figure 3a (open symbols) shows that the resistivity decreases (and conductivity increases) as a function of temperature up to 500°C. The filled symbols present the resistivity and conductivity after ramping the temperature down and show that the changes are irreversible. Zhong et al.

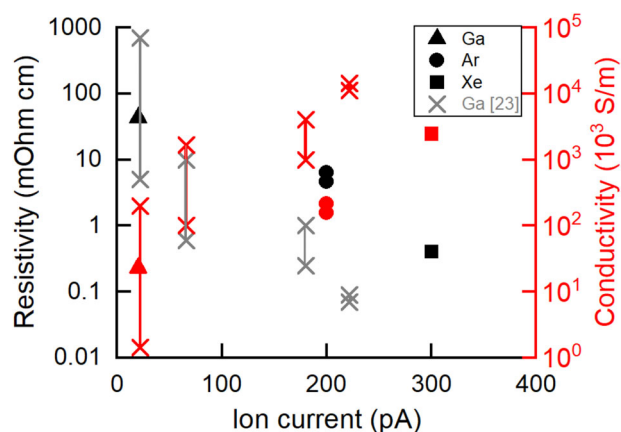


FIGURE 2 Resistivity (black and gray) and conductivity (red) as a function of ion current for IB deposited Pt. Data for Ga ions (triangles), Ar ions (circles) and Xe ions (squares) are compared to reference data (Tao et al., 1990) for Ga ions (X's). For the reference data the total ion dose was varied and the X's indicate the maximum and minimum values for each ion current.

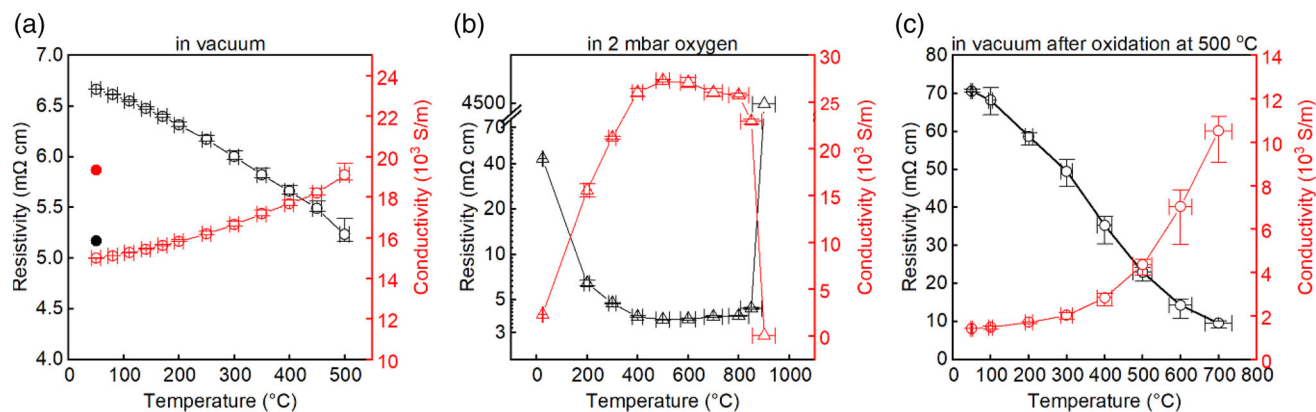


FIGURE 3 Resistivity (black) and conductivity (red) as function of a temperature for IB deposited Pt (a) Ar-IB, in vacuum, (b) Ga-IB, in 2 mbar O_2 in an ETEM and (c) Ar-IB, in vacuum after being heated to 500°C in ambient air. The filled circles in (a) presents the measured values after ramping the temperature down.

observed a similar but much more pronounced trend for EB deposited Pt with approximately 10^3 times larger decrease in resistivity within the same temperature range (Zhong et al., 2020). They explained the temperature dependence by Pt crystallization and grain growth (Zhong et al., 2020), leading to lower tortuosity and possibly lower porosity.

Below 500°C, supported Pt nanoparticles are known to be relatively stable and the particle growth is not likely due to Ostwald ripening or particle migration (Löf et al., 1993; Simonsen et al., 2010, 2011, 2012, 2017). The Pt particle growth could instead be due to the coalescence of Pt nanoparticles already in physical contact (Asoro et al., 2010; Wynblatt & Gjostein, 1976), and perhaps due to further decomposition of deposited Pt precursor.

When using deposited Pt as electrical contacting material, it is important that the resistivity is stable within the measuring conditions. According to Figure 3a, the resistivity stays within approx. 1 m Ω cm over a temperature range of approx. 500 °C. Larger changes in the measured resistivity of a sample connected to the electrodes with IB deposited Pt can, therefore, be attributed to the actual sample and not to changes in the contacting material.

3.3 | Low oxygen pressure

In some cases, *operando* microscopy experiments are conducted in reactive gases (Ma et al., 2023). In an oxidizing environment, it can be expected that the hydrocarbon matrix and the surface of Pt will oxidize (Van Spronsen et al., 2017). The conductivity of IB deposited Pt (GaPt in Table 1) was investigated in an ETEM in 2 mbar O_2 . Figure 3b shows that the decrease in resistivity (and increase in conductivity) in 2 mbar O_2 up to 500°C is approximately 10 times larger than that in vacuum. At the temperatures above 500°C, the resistivity is relatively stable, until 900°C where it increases by a factor of about 10^3 .

Figure 4 presents EELS spectra in the energy range of the carbon edge (284 eV) recorded during the same experiment as presented by

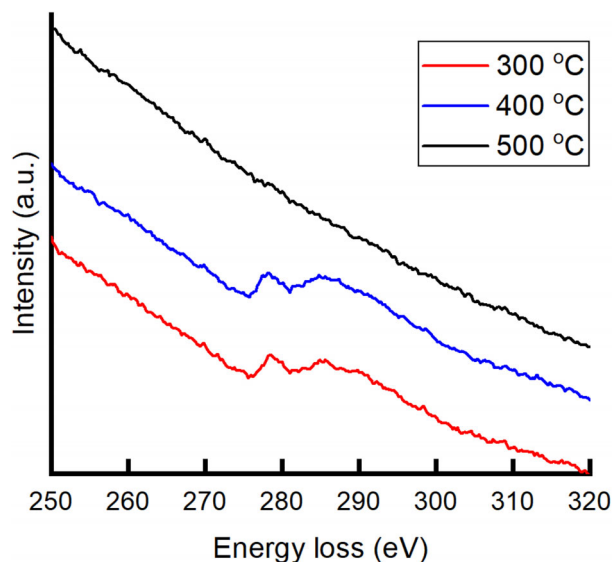


FIGURE 4 EELS spectra of Ga IB deposited Pt recorded at 300–500°C in 2 mbar O₂. The spectra energy range is chosen to show the C K-edge. The spectra are shifted relative to each other on the y-axis to avoid overlap.

Figure 3b. The spectra show the presence of carbon in the sample at 300 and 400°C, while the carbon has been fully removed at 500°C. The sample was kept at 500°C for 25 min before the EELS spectrum was recorded. This shows that the hydrocarbon matrix is removed by thermal oxidation, and that metallic Pt remains as the contacting material.

The drastic increase in resistivity at 900°C (Figure 3b) is, therefore, not related to changes in the hydrocarbon matrix but must be associated with changes in the Pt nanostructure. This is supported by the ETEM images recorded in the same experiment (Figure 5). Up to 800°C, the nanostructure of the deposited Pt appears to be relatively stable, despite the removal of the hydrocarbon matrix at 500°C. At 850°C, and more pronounced at 900°C, Pt coarsening is observed as larger structures appear and larger contrast differences indicate regions with varying density of Pt. Since no Pt is added to the sample during the experiment, the Pt added to the denser regions must have migrated from other areas which leads to increased tortuosity.

The results in Figures 3 and 5 show that IB-deposited Pt is relatively stable in O₂ at temperatures up to 800°C both in terms of structure and conductivity. This means that IB-deposited Pt can be used as electrical contacting material for *operando* microscopy experiments in oxidizing gasses and up to approx. 800–850°C. Above this temperature, the IB deposited Pt is not stable in O₂ and the electrical measurements are likely to be influenced by the drastic resistance increase in the contacting material.

3.4 | High oxygen pressure

Although Pt is a noble metal, it is known that nanostructured Pt can surface oxidize (Van Spronsen et al., 2017). In our case, where the

electrical contacting material consists of connected Pt nanodomains, such surface oxidation may influence the overall conductivity. The ETEM experiment presented in the previous section was conducted in a relatively low oxygen pressure of 2 mbar. In this section, we present how the Pt conductivity is influenced when the oxygen pressure is increased by a factor of 100.

To investigate this, the in-situ SEM experiment presented in Figure 3a was stopped after reaching 500°C, the in-situ stage was removed from the SEM, the temperature was raised to 500°C and kept for about 20 min in ambient air. Figure 3c shows the temperature dependence of the resistivity (and conductivity) in the vacuum of the SEM after this treatment.

Interestingly, the oxidation in the higher oxygen concentration led to an increase in the resistivity by a factor of 10 (comparing Figure 3a,c). Complete removal of the hydrocarbon component is anticipated to occur with the treatment in air (Figure 4). The observed change must, therefore, be related to the Pt component and/or the film micro- and nanostructure. A treatment in 210 mbar O₂ will not lead to bulk oxidation of Pt, but it is known that surface-oxidation will take place (Van Spronsen et al., 2017). It is likely that the higher O₂ concentration when heating in ambient air, leads to Pt surface oxidation to an extent that it worsens the electrical connections between metallic Pt nanodomains.

In conclusion, Figure 3 shows that in vacuum a pretreatment at 500°C can stabilize the conductivity of IB deposited Pt. A similar pretreatment in ambient air will not stabilize the conductivity of IB deposited Pt, if the following *operando* experiment is to be carried out in vacuum.

3.5 | Influence on conductivity from joule heating

In the previous section, we found that the IB-deposited Pt is relatively stable as electronic contacting material at temperatures up to approx. 800–850°C. This is, however, only when Joule heating from the electrical current in the Pt is not considered. In this section, we study the effect of electric current on the stability of the film.

In the vacuum of the SEM, films of deposited Pt (ArPt in Table 1) were exposed to a stepwise increase in the applied electrical current until a sudden decrease in electrical conductivity was observed. This was done for two different films: one kept at room temperature and one at 800°C, just below the temperature where the IB-deposited Pt becomes unstable in 2 mbar O₂ according to Figure 3b.

Figure 6 presents the measured resistivity (and conductivity) as a function of current density at RT and at 800°C. At RT, the resistivity is relatively stable for current densities up to approx. 100 kA/cm². At higher current densities, the resistivity decreases until a sudden increase at approx. 320 kA/cm². On the basis of the temperature dependence of the resistivity (Figure 3), this behavior can be attributed to the influence of Joule heating.

An SEM image was recorded for each step in applied current, showing no structural changes until reaching 320 kA/cm². Figure 7 shows that the structure changed significantly when going from

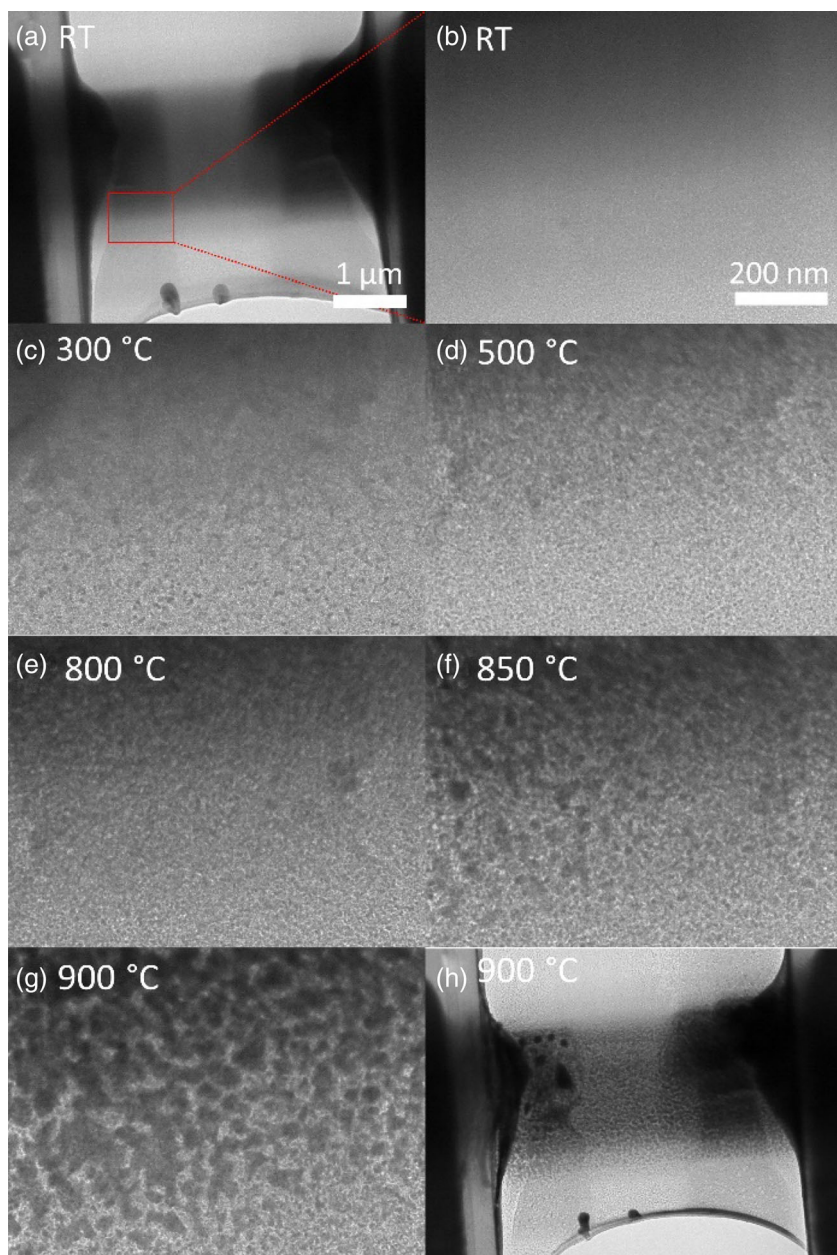


FIGURE 5 (a) Presents a TEM image of Ga IB deposited Pt. (b–g) Presents TEM images of the sample region marked by a red box in (a) as a function of temperature in 2 mbar O₂. The images are recorded approx. 5 min after reaching the indicated temperatures. (h) presents a TEM image recorded at 900 °C and at the same magnification as (a).

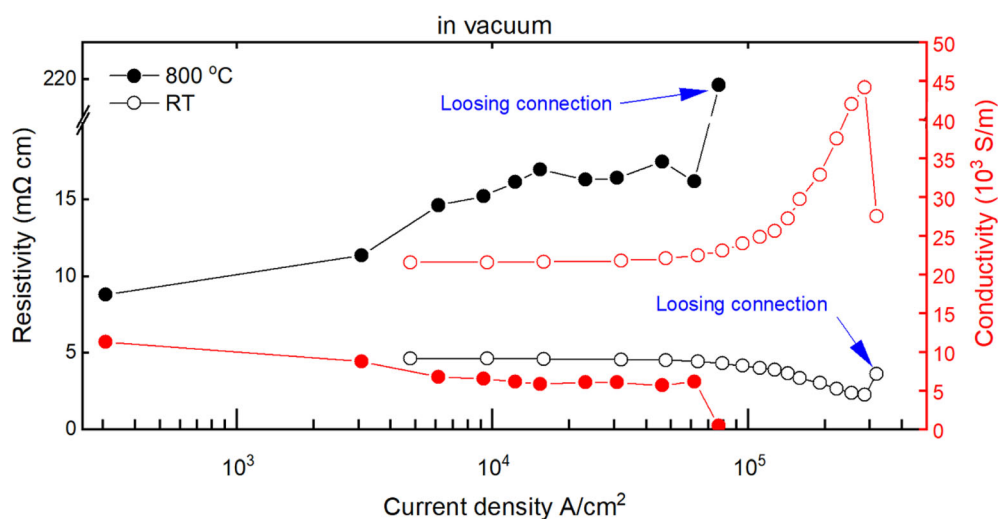


FIGURE 6 Resistivity (black) and conductivity (red) as function of applied current density through IB deposited Pt films measured in the vacuum of an SEM at RT (open symbols) and at 800 °C (filled symbols).

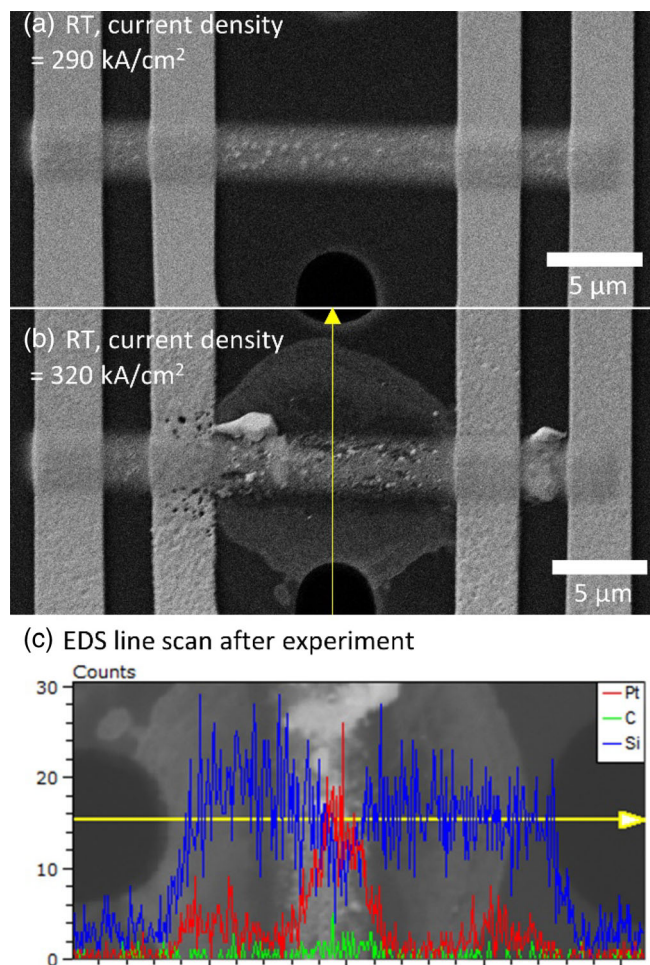


FIGURE 7 (a, b) SEM images of a MEMS chip with Ar IB deposited Pt recorded at RT when applying a current density of (a) 290 kA/cm² and (b) 320 kA/cm². (c) EDS line scan overlaid with an SEM image. The yellow lines in (b) and (c) indicate where the line scan was recorded.

290 to 320 kA/cm². Inhomogeneities and holes were also observed in the Pt chip electrodes when applying a current density of 320 kA/cm². Mele et al. performed a similar experiment using Ga IB deposited Pt and observed loss of electrical contact at approx. 500 kA/cm² (Mele et al., 2016), which is in the same order of magnitude to the value observed in the present study. EDS analysis (Figure 7c) shows that the bright pattern that appears around the film during exposure to a current density of 320 kA/cm² (Figure 7b) consists of Pt, apparently mobile in the heated region between the micro-electrode contacts that act as heat sink.

When raising the temperature via the heating element of the chip and Joule heating via an electric current through the deposited Pt, it can be expected that loss in the electrical connection will be observed at lower currents compared to RT. Indeed, as shown in Figure 6, the resistivity at 800°C is relatively stable only up to approx. 60 kA/cm², while it increases abruptly above this value.

From these results, we conclude that when using IB deposited Pt as electrical contacting material, the applied current densities should be kept below a few hundred kA/cm² to operate in a stable regime.

However, when the temperature is raised by a heating element on the chip, the maximum current density limit needs to be lowered. The higher the temperature, the lower the limit.

3.6 | Time and electron beam

Two limitations should be mentioned regarding the present results. The effect of time and of the electron beam has not been investigated in this study. Even though the IB deposited Pt was relatively stable at 800°C below approx. 60 kA/cm² or at RT below approx. 300 kA/cm², instability may have been observed if the experiments were performed over a longer time span as electromigration over time can cause disconnection (Baldini et al., 1993).

Also, it has been well-documented that Pt nanostructures are sensitive to effects of the electron beam and can easily be mistaken for thermal instabilities (Simonsen et al., 2010). In this study, the beam dose was minimized in the electron microscopes by only exposing the sample to the electron beam when images were recorded, and the beam was otherwise blanked. The images showed no signs of structural changes by the beam. However, it cannot be fully excluded that the electron beam had an effect which was not observed in the images, but nevertheless influenced the electrical measurements.

4 | CONCLUSION

IB deposited Pt is a good option as electrical contacting material when performing in-situ or *operando* electron microscopy in vacuum or in oxygen, and at temperatures of 20–800°C. The structure of the IB deposited Pt is relatively stable up to a temperature of approx. 800°C and up to an applied current density of approx. 100 kA/cm². The conductivity is observed to irreversibly increase as a function of temperature. This is mainly explained by thermally activated coarsening and densification of the nanostructured Pt. On the contrary, high temperature treatment in ambient conditions can deteriorate conductivity, likely by Pt surface oxidation.

The resistivity of IB deposited Pt films is generally high compared to good electronic conductors. For example, 10³–10⁵ times higher than that of bulk metallic Pt. This can make it challenging to conduct accurate measurements on highly conducting materials. The routes to lowering the resistance of the contacting material are (a) depositing thicker layers and (b) reducing the resistivity. The resistivity of the contacting material can be reduced by increasing the applied ion current during deposition and by thermal annealing at a temperature of 500°C in a few mbar of oxygen.

AUTHOR CONTRIBUTIONS

Søren Bredmose Simonsen: Conceptualization; investigation; funding acquisition; writing – original draft; methodology; validation; visualization; writing – review and editing; project administration; formal analysis; supervision; data curation; resources. **Zhongtao Ma:** Investigation; writing – review and editing; methodology; validation; visualization. **Elisabeth Mariegaard:** Investigation; writing – review

and editing; validation; methodology. **Salvatore De Angelis:** Supervision; writing – review and editing; investigation. **Waynah Lou Dacayan:** Investigation; writing – review and editing. **Kristian Speranza Mølhav:** Supervision; writing – review and editing. **Christodoulos Chatzichristodoulou:** Supervision; writing – review and editing.

ACKNOWLEDGMENTS

This project has received funding from the European Research Council (ERC) under the European Union's Horizon 2020 research and innovation programme (grant agreement No. 850850)."

DATA AVAILABILITY STATEMENT

The data that support the findings of this study are available from the corresponding author upon reasonable request.

ORCID

Søren Bredmose Simonsen  <https://orcid.org/0000-0001-7172-1225>

REFERENCES

- Alam, S. B., Andersen, C. R., Panciera, F., Nilausen, A. A. S., Hansen, O., Ross, F. M., & Mølhav, K. (2020). In situ TEM modification of individual silicon nanowires and their charge transport mechanisms. *Nanotechnology*, 31, 494002. <https://doi.org/10.1088/1361-6528/ababc8>
- Allard, L. F., Bigelow, W. C., Jose-Yacamán, M., Nackashi, D. P., Damiano, J., & Mick, S. E. (2009). A new MEMS-based system for ultra-high-resolution imaging at elevated temperatures. *Microscopy Research and Technique*, 72, 208–215. <https://doi.org/10.1002/jemt.20673>
- Asoro, M. A., Kovar, D., Shao-Horn, Y., Allard, L. F., & Ferreira, P. J. (2010). Coalescence and sintering of Pt nanoparticles: *in situ* observation by aberration-corrected HAADF STEM. *Nanotechnology*, 21, 25701. <https://doi.org/10.1088/0957-4484/21/2/025701>
- Baldini, G. L., De Munari, I., Scorzoni, A., & Fantini, F. (1993). Electromigration in thin-films for microelectronics. *Microelectronics and Reliability*, 33, 1779–1805. [https://doi.org/10.1016/0026-2714\(93\)90086-E](https://doi.org/10.1016/0026-2714(93)90086-E)
- Basak, S., Dzieciol, K., Durmus, Y. E., Tempel, H., Kungl, H., George, C., Mayer, J., & Eichel, R.-A. (2022). Characterizing battery materials and electrodes via *in situ/operando* transmission electron microscopy. *Chemical Physics Reviews*, 3, 31303. <https://doi.org/10.1063/5.0075430>
- Blauner, P. G., Ro, S., Butt, Y., & Melngailis, J. (1989). Focused ion beam fabrication of submicron gold structures. *Journal of Vacuum Science & Technology B: Microelectronics and Nanometer Structures*, 7, 609. <https://doi.org/10.1116/1.584803>
- Creemer, J. F., Helveg, S., Kooyman, P. J., Molenbroek, A. M., Zandbergen, H. W., & Sarro, P. M. (2010). A MEMS reactor for atomic-scale microscopy of nanomaterials under industrially relevant conditions. *Journal of Microelectromechanical Systems*, 19, 254–264. <https://doi.org/10.1109/JMEMS.2010.2041190>
- Della Ratta, A. D., Melngailis, J., & Thompson, C. V. (1993). Focused-ion beam induced deposition of copper. *Journal of Vacuum Science & Technology B: Microelectronics and Nanometer Structures*, 11, 2195. <https://doi.org/10.1116/1.586455>
- Evans, S. A., Bartelt, J. L., Sloan, B. J., & Varnell, G. L. (1978). Fabrication of integrated injection logic using E-beam lithography. *Journal of Vacuum Science and Technology*, 15, 969–972. <https://doi.org/10.1116/1.569687>
- Furuya, K. (2008). Nanofabrication by advanced electron microscopy using intense and focused beam. *Science and Technology of Advanced Materials*, 9, 14110. <https://doi.org/10.1088/1468-6996/9/1/014110>
- Gamo, K., Takakura, N., Takehara, D., & Namba, S. (1984). Characteristics of selective deposition of metal organic films using focused ion beams. *Conference on Solid State Devices and Materials*, 31–34. <https://doi.org/10.7567/ssdm.1984.a-2-5>
- Gamo, K., Takehara, D., Hamamura, Y., Tomita, M., & Namba, S. (1986). Maskless ion beam assisted deposition of W and Ta films. *Microelectronic Engineering*, 5, 163–170. [https://doi.org/10.1016/0167-9317\(86\)90043-2](https://doi.org/10.1016/0167-9317(86)90043-2)
- Gaulandris, F., Simonsen, S. B., Wagner, J. B., Mølhav, K., Muto, S., & Kuhn, L. T. (2020). Methods for calibration of specimen temperature during *in situ* transmission electron microscopy experiments. *Microscopy and Microanalysis*, 26, 3–17. <https://doi.org/10.1017/S1431927619015344>
- Gross, M. E., Brown, W. L., Linnros, J., Harriott, L. R., Cummings, K. D., & Funsten, H. O. (1986). Photon and ion beam-induced chemistry of palladium acetate films. *MRS Online Proceedings Library*, 75, 91–97. <https://doi.org/10.1557/PROC-75-91>
- Haas, B., Rouvière, J. L., Boureau, V., Berthier, R., & Cooper, D. (2019). Direct comparison of off-axis holography and differential phase contrast for the mapping of electric fields in semiconductors by transmission electron microscopy. *Ultramicroscopy*, 198, 58–72. <https://doi.org/10.1016/J.ULTRAMIC.2018.12.003>
- Hammad Fawey, M., Chakravadhanula, V. S. K., Reddy, M. A., Rongeat, C., Scherer, T., Hahn, H., Fichtner, M., & Kübel, C. (2016). In situ TEM studies of micron-sized all-solid-state fluoride ion batteries: Preparation, prospects, and challenges. *Microscopy Research and Technique*, 79, 615–624. <https://doi.org/10.1002/jemt.22675>
- Hansen, T., Wagner, J., Jinschek, J., & Dunin-Borkowski, R. (2009). The titan environmental transmission electron microscope: Specifications, considerations and first results. *Microscopy and Microanalysis*, 15, 714–715. <https://doi.org/10.1017/S1431927609097396>
- Kamaladasa, R. J., Sharma, A. A., Lai, Y.-T., Chen, W., Salvador, P. A., Bain, J. A., Skowronski, M., & Picard, Y. N. (2015). *In situ* TEM imaging of defect dynamics under electrical bias in resistive switching rutile-TiO₂. *Microscopy and Microanalysis*, 21, 140–153. <https://doi.org/10.1017/S1431927614013555>
- Komano, H., Ogawa, Y., & Takigawa, T. (1989). Silicon oxide film formation by focused ion beam (FIB)-assisted deposition. *Japanese Journal of Applied Physics*, 28, 2372–2375. <https://doi.org/10.1143/JJAP.28.2372>
- Lööf, P., Stenbom, B., Nordén, H., & Kasemo, B. (1993). Rapid sintering in NO of nanometre-sized Pt particles on gamma-Al₂O₃ Observed by CO temperature-programmed desorption and transmission electron microscopy. *Journal of Catalysis*, 144, 60–76. <https://doi.org/10.1006/jcat.1993.1314>
- Ma, Z., Lou Dacayan, W., Chatzichristodoulou, C., Mølhav, K. S., Chiabrera, F. M., Zhang, W. A., & Simonsen, S. B. (2023). Electrochemical impedance spectroscopy integrated with environmental transmission electron microscopy. *Small Methods*, 2201713. <https://doi.org/10.1002/smt.202201713>
- Mele, L., Konings, S., Dona, P., Evertz, F., Mitterbauer, C., Faber, P., Schampers, R., & Jinschek, J. R. (2016). A MEMS-based heating holder for the direct imaging of simultaneous *in-situ* heating and biasing experiments in scanning/transmission electron microscopes. *Microscopy Research and Technique*, 79, 239–250. <https://doi.org/10.1002/jemt.22623>
- Mølhav, K., Madsen, D. N., Dohn, S., & Bøggild, P. (2004). Constructing, connecting and soldering nanostructures by environmental electron beam deposition. *Nanotechnology*, 15, 1047–1053. <https://doi.org/10.1088/0957-4484/15/8/033>
- Niekiel, F., Kraschewski, S. M., Müller, J., Butz, B., & Spiecker, E. (2017). Local temperature measurement in TEM by parallel beam electron diffraction. *Ultramicroscopy*, 176, 161–169. <https://doi.org/10.1016/j.ultramicro.2016.11.028>
- Protochips. (2017). Sample Prep Fib Sample Preparation. <http://www.protochips.com/wp-content/uploads/2017/10/prep-fib-samples.pdf>
- Puretz, J., & Swanson, L. W. (1992). Focused ion beam deposition of Pt containing films. *Journal of Vacuum Science & Technology B: Microelectronics and Nanometer Structures*, 10, 1047–1053. <https://doi.org/10.1116/1.584803>

- Microelectronics and Nanometer Structures*, 10, 2695. <https://doi.org/10.1116/1.586028>
- Ro, J. S., Dubner, A. D., Thompson, C. V., & Melngailis, J. (1987). Microstructure of gold films grown by ion induced deposition. *MRS Proceedings*, 101, 255. <https://doi.org/10.1557/PROC-101-255>
- Schwarzbach, D., Gonzalez-Julian, J., Guillon, O., Roddatis, V., & Volkert, C. A. (2019). Towards In-situ electron microscopy studies of flash sintering. *Ceramics*, 2, 472–487. <https://doi.org/10.3390/ceramics2030036>
- Seeger, A., Paulson, S., Falvo, M., Helser, A., Li, R. M. T., Superfine, R., & Washburn, S. (2001). Hands-on tools for nanotechnology, Cit. *Journal of Vacuum Science & Technology B: Microelectronics and Nanometer Structures Processing*, 19, 2717. <https://doi.org/10.1116/1.1412890>
- Simonsen, S. B., Chorkendorff, I., Dahl, S., Skoglundh, M., Meinander, K., Jensen, T. N., Lauritsen, J. V., & Helveg, S. (2012). Effect of particle morphology on the ripening of supported Pt nanoparticles. *Journal of Physical Chemistry C*, 116, 5646–5653. <https://doi.org/10.1021/jp2098262>
- Simonsen, S. B., Chorkendorff, I., Dahl, S., Skoglundh, M., Sehested, J., & Helveg, S. (2010). Direct observations of oxygen-induced platinum nanoparticle ripening studied by in situ TEM. *Journal of the American Chemical Society*, 132, 7968–7975. <https://doi.org/10.1021/ja910094r>
- Simonsen, S. B., Chorkendorff, I., Dahl, S., Skoglundh, M., Sehested, J., & Helveg, S. (2011). Ostwald ripening in a Pt/SiO₂ model catalyst studied by in situ TEM. *Journal of Catalysis*, 281, 147–155. <https://doi.org/10.1016/j.jcat.2011.04.011>
- Simonsen, S. B., Wang, Y., Jensen, J. O., & Zhang, W. (2017). Coarsening of carbon black supported Pt nanoparticles in hydrogen. *Nanotechnology*, 28, 475710. <https://doi.org/10.1088/1361-6528/aa91a8>
- Tao, T., Ro, J., Melngailis, J., Xue, Z., & Kaesz, H. D. (1990). Focused ion beam induced deposition of platinum. *Journal of Vacuum Science & Technology B: Microelectronics and Nanometer Structures*, 8, 1826. <https://doi.org/10.1116/1.585167>
- Tjaden, B., Cooper, S. J., Brett, D. J., Kramer, D., & Shearing, P. R. (2016). On the origin and application of the Bruggeman correlation for analysing transport phenomena in electrochemical systems. *Current Opinion in Chemical Engineering*, 12, 44–51. <https://doi.org/10.1016/j.coche.2016.02.006>
- Van Leer, B., Wang, Y.-C., & Ciannuzzi, L. A. (2009). Protective carbon deposition for superior FIB prepared (S)TEM specimens. *Microscopy and Microanalysis*, 15, 336–337. <https://doi.org/10.1017/S1431927609093428>
- Van Spronsen, M. A., Frenken, J. W. M., & Groot, I. M. N. (2017). Observing the oxidation of platinum. *Nature Communications*, 8, 429. <https://doi.org/10.1038/s41467-017-00643-z>
- Vijayan, S., & Aindow, M. (2019). Temperature calibration of TEM specimen heating holders by isothermal sublimation of silver nanocubes. *Ultramicroscopy*, 196, 142–153. <https://doi.org/10.1016/j.ultramic.2018.10.011>
- Wang, Z., Tang, Y., Zhang, L., Li, M., Shan, Z., & Huang, J. (2020). In situ TEM observations of discharging/charging of solid-state lithium-sulfur batteries at high temperatures. *Small*, 16, 2001899. <https://doi.org/10.1002/sml.202001899>
- Wynblatt, P., & Gjostein, N. A. (1976). Supported metal crystallites. *Progress in Solid State Chemistry*, 9, 21–58. [https://doi.org/10.1016/0079-6786\(75\)90013-8](https://doi.org/10.1016/0079-6786(75)90013-8)
- Xu, Z., Kosugi, T., Gamo, K., & Namba, S. (1989). An x-ray photoelectron spectroscopy study on ion beam induced deposition of tungsten using WF₆. *Journal of Vacuum Science & Technology B: Microelectronics and Nanometer Structures*, 7, 1959. <https://doi.org/10.1116/1.584656>
- Yang, Z., Zhu, Z., Ma, J., Xiao, D., Kui, X., Yao, Y., Yu, R., Wei, X., Gu, L., Hu, Y.-S., Li, H., Zhang, X., Yang, Z., Ma, J., Xiao, D., Yao, Y., Yu, R., Gu, L., Hu, Y., ... Wei, X. (2016). Phase separation of Li₂S/S at nanoscale during electrochemical lithiation of the solid-state lithium-sulfur battery using In situ TEM. *Advanced Energy Materials*, 6, 1600806. <https://doi.org/10.1002/aenm.201600806>
- Yokosawa, T., Alan, T., Pandraud, G., Dam, B., & Zandbergen, H. (2012). In situ TEM on (de)hydrogenation of Pd at 0.5–4.5 bar hydrogen pressure and 20–400°C. *Ultramicroscopy*, 112, 47–52. <https://doi.org/10.1016/j.ultramic.2011.10.010>
- Young, R. J., & Puret, J. (1995). Focused ion beam insulator deposition. *Journal of Vacuum Science & Technology B: Microelectronics and Nanometer Structures*, 13, 2576. <https://doi.org/10.1116/1.588026>
- Zhang, Z., Wang, Z., Zhang, L., Liu, D., Yu, C., Yan, X., Xie, J., & Huang, J. (2022). Unraveling the conversion evolution on solid-state Na–SeS₂ battery via In situ TEM. *Advanced Science*, 9, 2200744. <https://doi.org/10.1002/advs.202200744>
- Zheng, H., Lu, X., & He, K. (2022). In situ transmission electron microscopy and artificial intelligence enabled data analytics for energy materials. *Journal of Energy Chemistry*, 68, 454–493. <https://doi.org/10.1016/j.jechem.2021.12.001>
- Zhong, C., Qi, R., Zheng, Y., Cheng, Y., Song, W., & Huang, R. (2020). The relationships of microscopic evolution to resistivity variation of a FIB-deposited platinum interconnector. *Micromachines*, 11, 588. <https://doi.org/10.3390/M111060588>
- Zintler, A., Kunz, U., Pivak, Y., Sharath, S. U., Vogel, S., Hildebrandt, E., Kleebe, H. J., Alff, L., & Molina-Luna, L. (2017). FIB based fabrication of an operative Pt/HfO₂/TiN device for resistive switching inside a transmission electron microscope. *Ultramicroscopy*, 181, 144–149. <https://doi.org/10.1016/j.ultramic.2017.04.008>

How to cite this article: Simonsen, S. B., Ma, Z., Mariegaard, E., De Angelis, S., Dacayan, W. L., Mølhave, K. S., & Chatzichristodoulou, C. (2023). Ion-beam deposited platinum as electrical contacting material in *operando* electron microscopy experiments at elevated temperatures. *Microscopy Research and Technique*, 86(8), 1003–1011. <https://doi.org/10.1002/jemt.24373>